Sustainable Development Research; Vol. 7, No. 2; 2025
ISSN 2690-9898 E-ISSN 2690-9901
https://doi.org/10.30560/sdr.v7n2p153

The Simulation of Gas Film Flow Field in Aerostatic Thrust Bearing

Zuxian Zhang[1] & Yujie Ren[2]

[1] China Institute of Water Resources and Hydropower Research, Beijing, China

[2] Jianke EET Co., Ltd., Beijing, China

Correspondence: Zuxian Zhang, China Institute of Water Resources and Hydropower Research, Beijing, China. Tel: 86-010-6878-1512. E-mail: zhangzx@iwhr.com

Received: May 18, 2025 Accepted: June 23, 2025 Online Published: June 25, 2025

Abstract

Based on the CFD software, the numerical simulation and visualization of the gas flow in the gas film gap are carried out. Considering the influence of gas flow, the laminar flow model was adopted when the clearance is relatively small and a realizable model was adopted for large gaps. This research analyzes the effect of bearing clearance on gas pressure, velocity and Mach number, and accurately captures the flow field characteristics of the bearing inlet region. The calculation results show that the inlet gas film pressure drops significantly or even lower than the ambient pressure under large clearance conditions, so the influence of inertial force cannot be ignored. The mechanism of pressure drop and recovery is revealed by the theory of expansion wave and compression wave for the phenomenon of shock wave near the entrance.

Keywords: power machinery, aerostatic bearing, numerical simulation, flow field distribution

1. Introduction

Aerostatic thrust bearings are sliding bearings that use gas as the lubricated medium. Because of its dry, clean and contamination-resistant properties, Aerostatic thrust bearings have more extensive applications. But in terms of its carrying capacity, it mainly used in high-speed or light-load rotating machinery. Increasing its carrying capacity is an important issue in the development of aerostatic thrust bearing (Yang et al, 2012). Experimental studies have found that there is an unexpected sudden drop in pressure at the bearing air inlet at the high gas supply pressure (Poupard & Drouin, 1973). In order to explain the mechanism of this abrupt pressure drop, experts and scholars have carried out a lot of research. HARUO MORI firstly proposed that this abrupt pressure drop is due to the positive shock within the gas film clearance in 1961 (Mori, 1961). HARUO MORI and Y.MIYAMATSU described all kinds of flow conditions causing the changes of pressure in 1969. This research not only described the gas state equation under different working conditions, but also classified the flow conditions simply (Mori & Miyamatsu, 1969). In 1982, R.S.Gupta and V.K.Kapur who studied the influence of the inertia force of the bearing indicated that inertial force lead to the drop of the film pressure at the entrance (Gupta & Kapur, 1982).

With the development of computer technology, scholars began using CFD to solve gas constraint equations to obtain a more accurate flow results (Yoshimoto et al, 2007). In 2009, Mohamed E.Eleshaky simulate full N-S equations of three-dimension and compressible turbulence by CFD, which calculate two kinds of bearing structures respectively and the results presented the process of formation of the shock at the entrance (Eleshaky, 2009).

Based on the previous research, this paper numerically simulates the gas film flow field of the aerostatic thrust bearings with the help of FLUENT software, and calculates the flow field characteristics in the gas film clearance of the bearing under different bearing clearances, and conducts a mechanism analysis of the flow field characteristics.

2. Model establishment

2.1 Control Equations

The conservative N-S governing equation is used to solve the three-dimensional and steady-state compressible flow. The expressions of each equation are:

$$\frac{\partial \rho}{\partial t}+\frac{\partial(\rho \mathrm{u}_i)}{\partial x_i}=0 \tag{1}$$

$$\frac{\partial}{\partial t}(\rho u_i)+\frac{\partial}{\partial x_j}(\rho u_i u_j)=-\frac{\partial p}{\partial x_i}+\frac{\partial}{\partial x_j}[\mu(\frac{\partial u_i}{\partial x_j}+\frac{\partial u_j}{\partial x_i}-\frac{2}{3}\delta_{ij}\frac{\partial u_j}{\partial x_j})]+\frac{\partial}{\partial x_j}(-\rho\overline{u_i' u_j'}) \tag{2}$$

$$\frac{\partial}{\partial x_i}[u_i(\rho E+p)]=\frac{\partial}{\partial x_i}[(\lambda+\frac{c_p\mu_t}{\Pr_t})\frac{\partial T}{\partial x_i}+u_i(\tau_{ij})] \tag{3}$$

Where

$$\rho\overline{u_i' u_j'}=\frac{2}{3}(\rho k+\mu_t\frac{\partial u_i}{\partial x_i})\ \sigma_{ij}-\mu_t(\frac{\partial u_i}{\partial x_j}+\frac{\partial u_j}{\partial xi}) \tag{4}$$

$$E=c_{p\frac{P}{\rho R}}-\frac{P}{\rho}+\frac{(u_1^{\ 2}+u_2^{\ 2}+u_3^{\ 2})}{2} \tag{5}$$

$$(\tau_{ij})=\mu(\frac{\partial u_j}{\partial x_i}+\frac{\partial u_i}{\partial x_j})-\frac{2}{3}\mu\frac{\partial u_i}{\partial x_i}\delta_{ij} \tag{6}$$

The flow of the medium is in a uniform state of thermodynamic equilibrium system, the equation of state acquired by the conservation of ideal gas law as follows:

$$P=\rho RT \tag{7}$$

$$P=(\gamma-1)\rho[e-\frac{(u_1^{\ 2}+u_2^{\ 2}+u_3^{\ 2})}{2}] \tag{8}$$

μ is molecular viscosity, determined by the Sutherland Law.

$$\frac{\mu}{\mu*}=(\frac{T}{T^*})^{3/2}\frac{T*+S}{T+S} \tag{9}$$

For air, μ*=1.716×10-5Pa.s, S=110.55K, T^*=273.11K.

2.2 Turbulence Equations

There are two main forms of fluid flow in the bearing gap, namely laminar flow and turbulent flow. For the turbulent state, this paper uses the realizable model and uses the enhanced wall function method to solve the turbulence equation. Transport equations of κ and ε are as follows:

equation of κ

$$\frac{\partial(\rho\kappa)}{\partial t}+\frac{\partial(\rho\kappa u_i)}{\partial x_i}=\frac{\partial}{\partial x_j}[\ (\mu+\frac{\mu_t}{\sigma_k})\frac{\partial k}{\partial x_j}]+G_k-\rho\varepsilon \tag{10}$$

equation of ε

$$\frac{\partial(\rho\varepsilon)}{\partial t}+\frac{\partial(\rho\varepsilon u_i)}{\partial x_i}=\frac{\partial}{\partial x_j}[(\mu+\frac{\mu_t}{\sigma_\varepsilon})\frac{\partial\varepsilon}{\partial x_j}]+\rho C_1 E\varepsilon-C_2\rho\frac{\varepsilon^2}{k+\sqrt{v\varepsilon}} \tag{11}$$

Where, σ_k=1.0, σ_ε=1.2, C_2=1.9.

The standard model has the potential to cause negative normal stresses in situations where the time-average strain rate is particularly large. In order for the flow to be more in line with the physical laws of turbulence, some constraints on the normal stress are required. In order to ensure this constraint, the literature Shih et al. (1995) believes that the coefficient Cμ in the turbulent viscosity calculation formula should not be a constant, but should be related to the strain rate.

2.3 Discrete and Meshing Area

The research object of this paper is a single-hole disc thrust bearing, whose structure is symmetrical. So this is simplified to a 1/4 model for calculation, and the schematic diagram is shown in Figure 1. The calculation area is meshed as shown in Figure 2. The model consists of three solid walls, one inlet, one outlet and two symmetry planes.

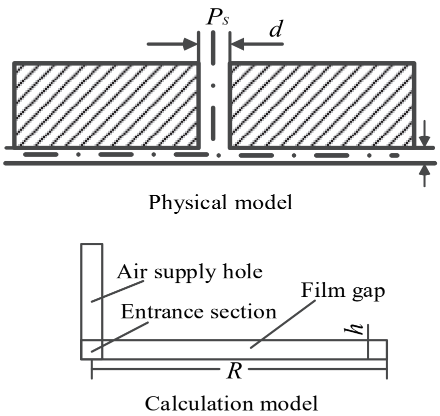

Figure 1. physical model

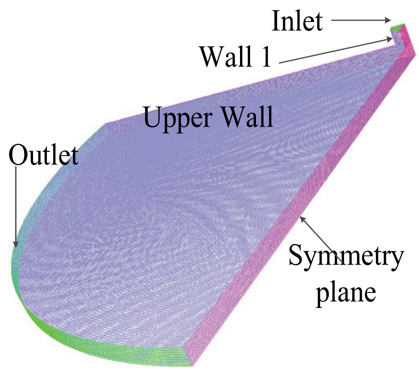

Figure 2. Schematic diagram of the discretization grid

2.4 Calculation Model

The numerical simulation software FLUENT is used to simulate the calculation, which is based on the density implicit separation method and uses the finite volume method to solve the governing equation and the turbulence equation in this paper. Considering the solution stability during simulation, the convection term in the equation adopts the first-order upwind style, and the diffusion term adopts the central difference format. The final convergence residuals are all set to 10^{-4}.

3. Calculation Results and Analysis

3.1 Calculation Results

Simulations are carried out at three different bore bearing clearances, namely A, B and C. The geometric parameters, mass flow and local Reynolds number of three different thrust bearing structures are given in Table 1.

Table 1. Different sizes of bearing clearance and its physical parameters

Type	*H*/mm	*d*/mm	*R*/mm	*P*/Mpa	Entrance—*Re*	Exit—*Re*	m/kg/s
A	0.06	0.85	25	0.8	306	13	0.03307
B	0.15	0.85	25	0.8	4022	138	0.36868
C	0.60	0.85	25	0.8	13816	469	1.26616

The ratio of the pressure along the radial direction to the ambient pressure at the ring surface of the thrust bearing with different clearances is shown in Figure 3. It can be seen that the bearing clearance has a great influence on the pressure change at the inlet of the throttle under the same supply pressure. When the bearing clearance is small, the outlet pressure at the outlet is reduced less and the pressure is slowly decreased along the boundary of the bearing. If it continues to increase the bearing clearance, the pressure at the outlet of the orifice is significantly reduced. When the bearing clearance reaches about 0.6mm, the pressure at the outlet of the orifice drops to atmospheric pressure. According to the velocity distribution along the radius direction as shown in Figure 4, the velocity distribution is opposite to the pressure at the inlet. When the bearing clearance is small, the bearing speed is also small.

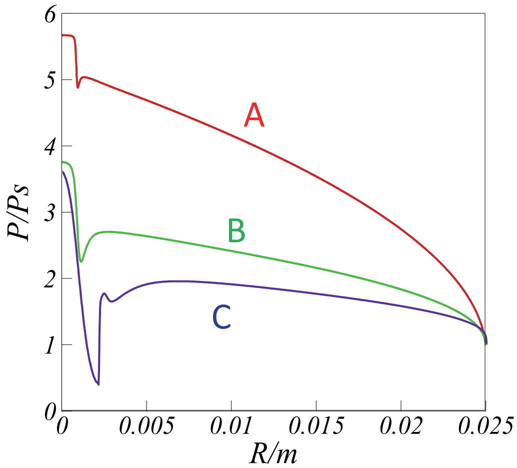

Figure 3. The pressure distribution along the radius direction

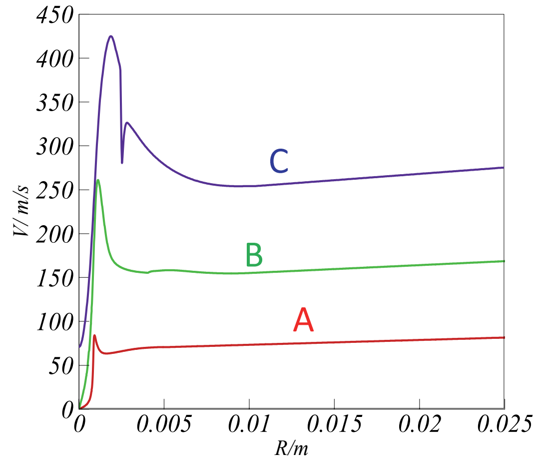

Figure 4. The velocity distribution along the radius direction

3.2 Result Analysis

3.2.1 Type A

When the flow of air through the orifice into the air gap, it will have complex flow field characteristics. Those flow field characteristics are related to gas state parameters of inlet and outlet, and even related to the flow path structure. The physical model shows the effect of viscous force and inertial force on gas pressure and velocity. The contour map of airflow field pressure, the contour map of Mach number and the diagram of velocity vector are illustrated in Figure 5 with the gas gap is 0.06 mm.

As shown in Figure 5-a, the Mach number of the airflow is less than 0.25. As shown in Figure 5-b, a vortex zone which is separated and decoupled is formed at the inlet of the gas film, and a reflux phenomenon occurs. When the gas flow from the inlet of the gas supply port to the section a-a of the cross-section, due to contract sharply of the flow cross section, the pressure decreases, and the velocity increases. The flow passage surface reaches the minimum at the section a-a of the cross-section, t, forming a throat, and at this time, the velocity reaches the maximum, forming a throat where the speed is maximized. As the fluid passes through the abruptly contracting passage, the streamline contracts and forms a minimal constriction at the throat due to inertial forces. It is obvious that the pressure at the upper wall of the corner is low, and the fluid continuously spreads to the wall surface which results in the formation of a vortex flow.

As shown in Figure 5-c, the distribution of velocity along the height of the center of the film is not symmetric near the air film inlet. The airflow velocity is fast near the lower bottom plate. Then, the distribution of velocity tends to be symmetrical after gradually moving away from the section a-a. The Re number calculated at the air film inlet is 306, and it is 13 at the outlet. It gets a conclusion that the flow state is laminar, where the inertial force of the airflow is relatively small and the viscous force plays a leading role in the process of flow. This flow model is called the pure viscous flow model, which satisfies the Reynolds equation in gas lubrication, and applied to gas bearings in majority working condition at present.

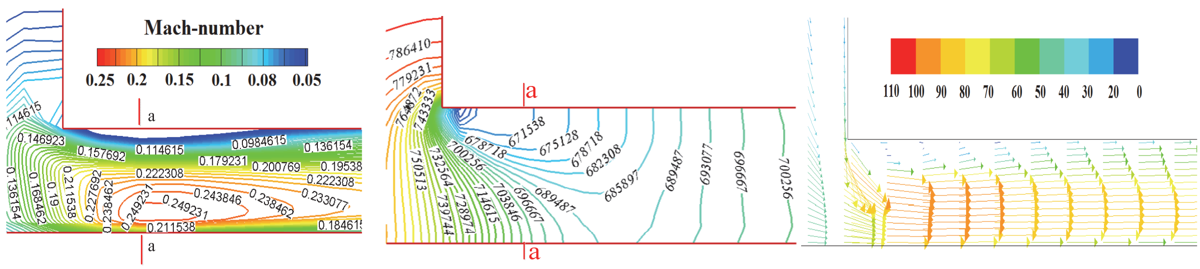

(a) The contour map of Mach number (b) The contour map of pressure (c) Speed vector

Figure 5. The internal view of type A thrust bearing flow field

3.2.2 Type B

The contour map of airflow field pressure, the contour map of Mach number and the diagram of velocity vector are illustrated in Figure 6 with the gas gap is 0.15 mm. When the airflow passes through the corner, as shown in Figure 6, the pressure suddenly drops, the Mach number increases sharply. The pressure at the throat section a-a is the smallest, and the Mach number reaches the maximum (about 0.8). The pressure starts to rise after the section a-a, as shown by curve B in Figure 3. The velocity begins to decrease significantly after section a-a, as shown by curve B in Figure 4. The reason is that as the gas flows from the inlet of the gas film to the throat, the pressure drops and the speed increases due to the contraction of the flow surface. The speed reaches the maximum at the throat which is in the subsonic state. Meanwhile, the inertial force acts strongly at this area. After the throat, a decelerating diffusion flow occurs due to an increase in the flow surface. Therefore, the pressure has picked up. As the speed decreases, the ratio of inertial force to viscous force gradually decreases. Therefore, the speed is greatly affected by the wall viscous force, resulting in a faster reduction.

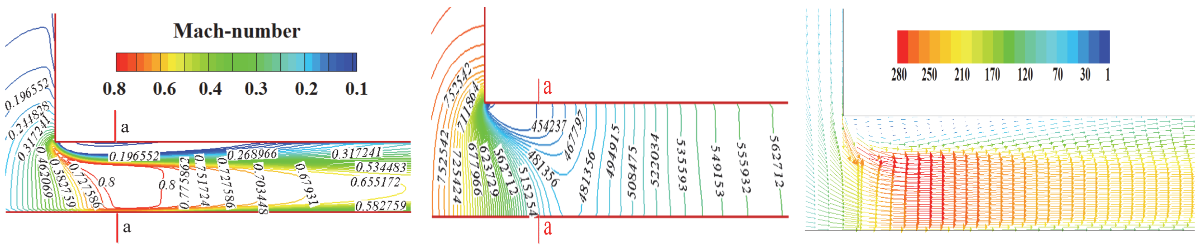

(a) The contour map of Mach number (b) The contour map of pressure (c) Speed vector

Figure 6. The internal view of type B thrust bearing flow field

3.2.3 Type C

The contour map of airflow field pressure, the contour map of Mach number and the diagram of velocity vector are illustrated in Figure 7 with the gas gap is 0.60 mm. It can be seen from Figure 7 that the Mach number of the airflow in the section a-a reaches 1. As the gas pressure drops, the speed increases, the subsonic flow transforms into the supersonic flow. The pressure continues to drop, even below ambient pressure, and the speed continues to rise after the airflow passes through section a-a. At the same time, the Mach number continues to increase. As the airflow passes through the ramp c-c, the pressure increases and the speed decreases. A discontinuous jump occurs in the pressure at section b-b, which results in a decrease in velocity discontinuity. After the airflow passes through section b-b, the pressure decreases again and the speed rises, as shown in Figure 8-a and Figure 8-b.

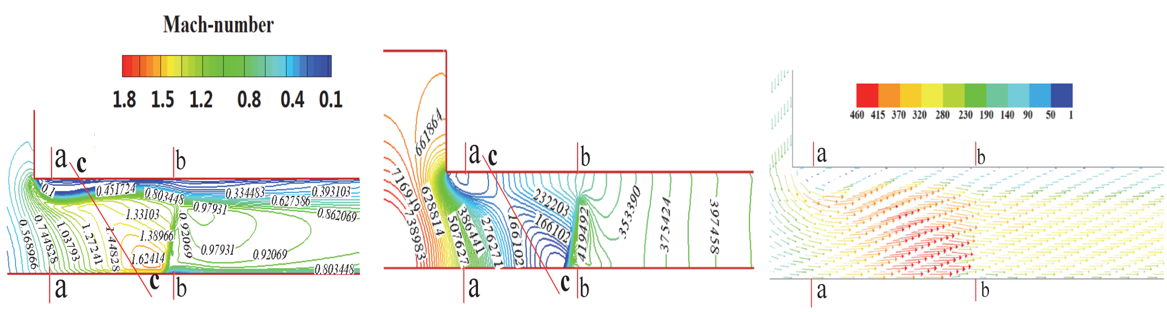

(a) The contour map of Mach number (b) The contour map of pressure (c) Speed vector

Figure 7. The internal view of type C thrust bearing flow field

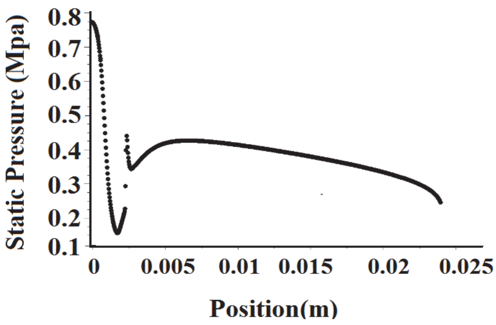

(a) Static pressure

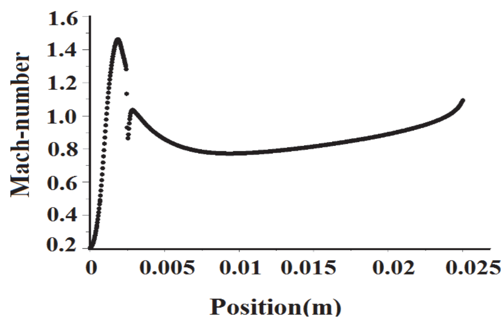

(b) Mach-number

Figure 8. Distribution of pressure and Mach number along the radius of the center of the film

3.2.4 Comprehensive Comparative Analysis Results

It can be seen from Figure 9 that the separation flow in a small region occurs in the upstream region of the inlet at the corner of air film. When the supersonic flow in the flow field passes through the convex of the separation zone, the expansion wave is formed. As the airflow passes through the position of the expansion wave, the airflow velocity at that location increases and the pressure decreases. While the airflow passes through the concave of the downstream in the separation zone, the compression wave is generated, which is continuously gathered to form the incident shock wave (such as the line AD in the Figure 9).

The flow forms in the boundary layer are divided into a supersonic flow and a subsonic flow. When the incident shock wave is incident on the bottom surface, as the incident shock wave can only extend to the supersonic flow at the boundary layer, the incident shock waves are reflected to the upper surface at the interface between the supersonic flow and the subsonic flow boundary of the boundary layer and gradually weakened as they reach the upper surface. The process is shown in Figure 9, where the line CD converges to EF.

The pressure is rising after the airflow passes through the incident shock wave. Due to the back pressure of the CD segment reflected wave to the bottom boundary layer, the pressure in this region increases. Then the flow rate is relatively lowered, the boundary layer is thickened, and the streamline is convex to form a separation zone.

As shown in the GB section of Figure 9, the supersonic fluid near the bottom surface region passes through the separation region to produce a weak compression wave that is gradually weakened during the process of reaching the upper surface. When the airflow reaches the concave surface of the downstream in the separation zone, an expansion wave is formed again. When the supersonic fluid passes through the expansion wave, the pressure decreases once again and the speed increases.

According to the Figure 7, a discontinuous mutation in pressure and velocity occurs at the b-b cross section. The reason is that a strong shock wave is generated in this section (as indicated at Figure 9). As a result, the supersonic fluid pressure in the bearing gap is lower than the ambient pressure at the bearing exit, and the supersonic flow is in state of accelerated when it is passing the expanded section. In order to achieve ambient pressure and avoid the form of the counter current airflow in the bearing gap, a strong shock wave is inevitably generated in the expansion section. In this process, the Mach number shows a fluctuation decrease in the flow radius direction, in addition, oscillating happens in the process of pressure ascending.

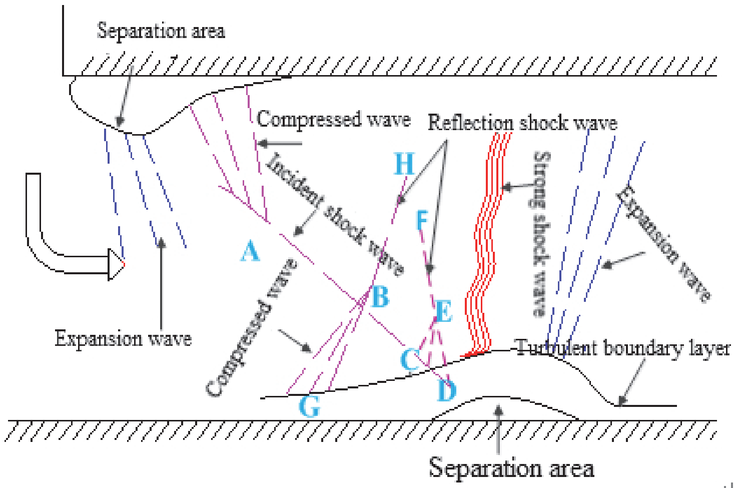

Figure 9. Interaction diagram between shock and boundary layer at the entrance

4. Conclusions

This paper analyzes complex flow field characteristics in aerostatic thrust bearing under different bearing clearances. The following conclusions are obtained:

(1) Bearing clearance affects the distribution of gas state parameters at the inlet;

(2) When the bearing clearance is small, the Mach number at the entrance of the throttle is less than 0.3. The viscous force plays a leading role, and the inertial force influence can be ignored;

(3) When the bearing clearance is large, the Mach number at the entrance of the throttle is greater than 0.3. The pressure at the entrance is significantly reduced, and the inertial force cannot be ignored;

(4) When the supersonic flow occurs at the entrance, the pressure firstly decreases even below the ambient pressure and then rises rapidly. The reasons for the pressure recovery are as follows:

a) The compression wave and the strong shock wave are generated in the bearing gap. After the shock wave, the speed decreases which lead to pressure recovery.

b) Because of the viscous force, the flow velocity near the wall is reduced. This phenomenon increase boundary layer thickness, reduce the center speed of the gap and increase the pressure.

References

Eleshaky, M. E. (2009). CFD investigation of pressure depressions in aerostatic circular thrust bearings. *Tribology International*, *42*(7), 1108–1117. https://doi.org/10.1016/j.triboint.2009.03.011

Gupta, R. S., & Kapur, V. K. (1982). Inertial effects on pressure depression in gas-lubricated thrust bearings. *Wear*, *77*(2), 203–206. https://doi.org/10.1016/0043-1648(82)90104-1

Mori, H. (1961). A theoretical investigation of pressure depression in externally pressurized gas-lubricated circular thrust bearings. *Journal of Basic Engineering*, *83*(2), 201–208. https://doi.org/10.1115/1.3658925

Mori, H., & Miyamatsu, Y. (1969). Theoretical flow-models for externally pressurized gas bearings. *Journal of Lubrication Technology*, *91*(1), 181–193. https://doi.org/10.1115/1.3554854

Poupard, M., & Drouin, G. (1973). Theoretical and experimental pressure distribution in supersonic domain for an inherently compensated circular thrust bearing. *Journal of Lubrication Technology*, *95*(2), 217–220. https://doi.org/10.1115/1.3451775

Shih, T. H., Liou, W. W., Shabbir, A., Yang, Z., & Zhu, J. (1995). A new k-ε eddy viscosity model for high Reynolds number turbulent flows. *Computers & Fluids*, *24*(3), 227–238. https://doi.org/10.1016/0045-7930(94)00032-T

Yang, J.-F., Chen, C., & Han, D.-J. (2012). Rotor-bearing system fluid-solid interaction and frequency modulation technology. *Journal of Vibration and Shock*, *31*(S), 281–285.

Yoshimoto, S., Yamamoto, M., & Toda, K. (2007). Numerical calculations of pressure distribution in the bearing clearance of circular aerostatic thrust bearings with a single air supply inlet. *Journal of Tribology*, *129*(2), 384–390. https://doi.org/10.1115/1.2464135

Copyrights

Copyright for this article is retained by the author(s), with first publication rights granted to the journal.

This is an open-access article distributed under the terms and conditions of the Creative Commons Attribution license (http://creativecommons.org/licenses/by/4.0/).